PERGAMON

Journal of Structural Geology 25 (2003) 541–555

JOURNAL OF STRUCTURAL GEOLOGY

www.elsevier.com/locate/jstrugeo

A record of crustal-scale stress; igneous foliation and lineation in the Mount Waldo Pluton, Waldo County, Maine

Caitlin N. Callahan, Michelle J. Markley*

Department of Earth and Environment, Mount Holyoke College, South Hadley, MA 01075, USA

Received 11 April 2001; accepted 11 April 2002

Abstract

The Late Devonian Mount Waldo pluton is a porphyritic granite that has a magmatic foliation and lineation. Foliation is defined by: (1) preferred orientation of potassium feldspar phenocrysts and biotite crystals, and (2) the anisotropy of magnetic susceptibility (AMS). AMS alone defines the lineation. The carrier of the AMS signal is multidomain magnetite, confirmed by petrographic observation, high bulk susceptibility (generally >3 E3 SI units) of samples, and results of isothermal remanent magnetization experiments. AMS data from 26 sites in the pluton consistently show a subhorizontal north–south-trending lineation (defined by the orientation of the maximum axis of the AMS ellipsoid) and a subvertical north–south-striking foliation (whose pole is the minimum axis of the AMS ellipsoid). At individual sites, the feldspar and AMS foliations are parallel. The lack of evidence for significant solid state deformation in the pluton suggests that both the lineation and foliation are entirely magmatic in origin. The pluton's relatively small size (15 km diameter) and shallow emplacement depth (≤ 3 kbar) suggest that it was in its magmatic state for a short time, probably less than one million years. The orientation of the lineation and foliation is consistent with their formation due to a small increment of crustal-scale strain absorbed by the pluton in its geologically brief magmatic state. If so, these fabrics record a Late Devonian crustal-scale strike-slip stress regime that may also have driven dextral movement on the neighboring Norumbega Fault Zone.

Keywords: Fabric; Magnetic susceptibility; Maine; Norumbega fault zone; Plutons; Stress

1. Introduction

Magmatic fabric in plutons commonly relates to regional crustal kinematics and local magmatic flow during pluton emplacement and crystallization (Balk, 1937; Bouchez, 1997; Benn et al., 1998; Paterson et al., 1998). In a review of the significance of magmatic fabrics in plutons, Paterson et al. (1998) noted that two end-member observations are common. When magmatic foliation in a pluton parallels the contact with the wall rock, the fabric is 'decoupled' and probably records magma chamber processes active during its crystallization or the late stages of pluton emplacement. When a magmatic foliation shows the same orientation regardless of its position in the pluton, it may be 'coupled' to regional tectonic deformation. In this second case, a pluton may provide a record of the regional kinematic history of the Earth's crust.

The goal of this study is to test the hypothesis that magmatic fabric in the Mount Waldo pluton preserved a record of crustal-scale kinematic activity at the time of its emplacement. Our study area is the Coastal Magmatic Province of Maine in the heart of the Northern Appalachian Mountains (Fig. 1). In this region (Fig. 2), three crustal-scale fault zones that were active during various stages of Paleozoic Appalachian mountain building are deeply eroded. Late Devonian intrusion of the Mount Waldo pluton stitched together two of these major faults (Stewart et al., 1995). The pluton also intruded adjacent to the third: the Norumbega Fault Zone (Fig. 2), whose kinematic history has been the subject of debate (see a recent volume edited by Ludman and West, 1999). In particular, transpression during the Devonian Acadian orogeny and later strike-slip faulting during the Carboniferous are well documented for the Norumbega (West and Lux, 1993; West, 1999; Ludman, 1999), but its kinematic history during the time between these two episodes of deformation is poorly constrained. The Mount Waldo pluton intruded the middle to upper crust during this poorly constrained time period (Stewart et al., 1995) and shows a strong magmatic fabric (Trefethen, 1944) that appears 'coupled' to regional deformation.

* Corresponding author. Tel.: +1-413-538-2814; fax: +1-413-538-2239.
E-mail address: mmarkley@mtholyoke.edu (M.J. Markley).

0191-8141/03/$ - see front matter © 2002 Elsevier Science Ltd. All rights reserved.
PII: S0191-8141(02)00052-4

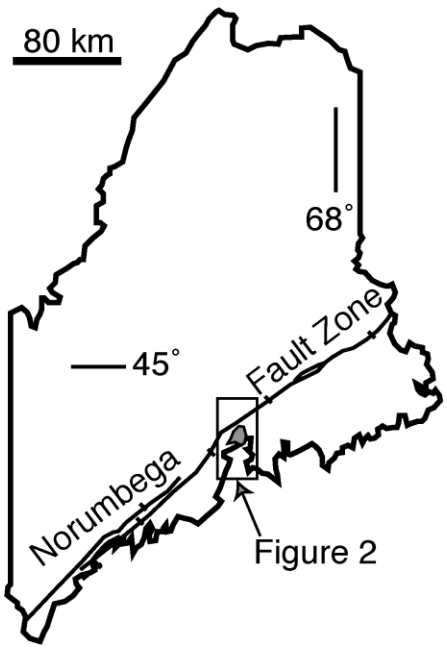

Fig. 1. The outline of the state of Maine provides a location for the study. The Norumbega Fault Zone accommodated dextral slip from the Devonian to the Carboniferous (West, 1999). East of this fault zone is the Coastal Maine Magmatic Province, characterized by Silurian and Devonian magmatic activity. The Late Devonian Mount Waldo pluton, the focus of this study, is shaded.

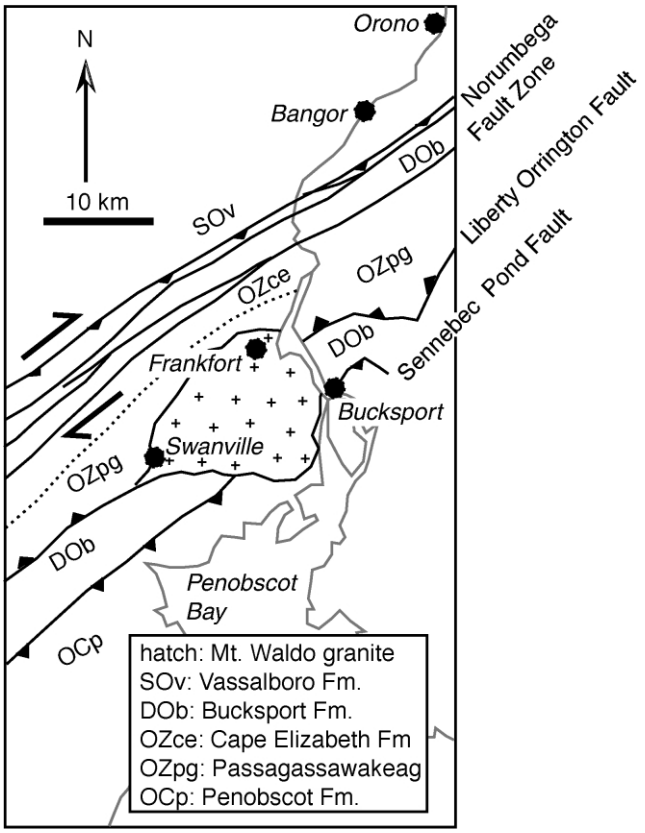

Fig. 2. Geologic map of the study area after Osberg et al. (1985) and Wones (1991). See Fig. 1 for location. The Mount Waldo pluton, the focus of this study, is a late Devonian granite. Ordovician to Devonian wall rock units are mainly metasediments that have been deformed at amphibolite and greenschist grade. The Sennebec Pond Fault is a suture zone (Stewart et al., 1995), the Liberty–Orrington Fault is a terrane boundary (Short, 2000), and the Norumbega Fault Zone has a 100-m.y.-long history of transpression and strike-slip (Ludman and West, 1999).

We report the orientation of foliation and lineation, as defined by the orientations of feldspar phenocrysts and anisotropy of magnetic susceptibility, in the Mount Waldo pluton. No evidence exists for solid state deformation of the pluton (Trefethen, 1944; Lux and Good, 2001), and foliation and lineation appear to be entirely magmatic in origin. We argue that foliation and lineation record a sort of 'snap-shot' of Late Devonian deformation kinematics in the region. These fabrics formed during an increment of crustal-scale strain absorbed by the pluton as it was crystallizing but still partially molten. Throughout the pluton, lineation is subhorizontal and trends north–south. Foliation is subvertical and strikes north–south. We interpret lineation as a record of the minimum principal stress, and the pole to foliation as a record of the maximum principal stress in the Late Devonian crust. This interpretation is consistent with the strike-slip tectonic regime (with intermediate principal stress vertical) that drove dextral strike-slip movement in the neighboring Norumbega Fault Zone.

2. Geologic background

2.1. Mount Waldo granite

The Mount Waldo pluton (Fig. 3) is a medium-grained, porphyritic, biotite granite (Trefethen, 1944). It contains potassium feldspar (50%), quartz (25%), plagioclase feldspar (20%), and biotite (5%). Both porphyritic and equigranular facies occur. Accessory minerals include hornblende, muscovite, titanite, tourmaline, and magnetite. Potassium feldspar crystals generally occur as euhedral phenocrysts ranging in length up to 6 cm and showing Carlsbad twinning and poikilitic inclusions of quartz and biotite. Lux et al. (2000) reported rapakivi textures on some feldspar phenocrysts. Quartz and feldspar crystals in the groundmass range in size from 5 to 10 mm. Plagioclase composition varies from An_9 to An_{19} (Sweeney, 1972). Plagioclase crystals are mostly subhedral, twinned, and show some zoning. Quartz crystals are subhedral with some undulose extinction and subgrain texture, but they are equant and lack a crystallographic preferred orientation (Fig. 3b). Magnetite is intergrown with 0.5–5 mm long biotite crystals (Fig. 3a). Thin dikes of aplite and pegmatite locally cut the granite.

The pluton also displays three mesoscale features whose origins suggest a dynamic magma chamber: a foliation defined by aligned potassium feldspar phenocrysts (Fig. 4), enclaves, and schlieren.

The first feature, the feldspar foliation, was first described and mapped by Trefethen (1944), who called it a 'plane flow'

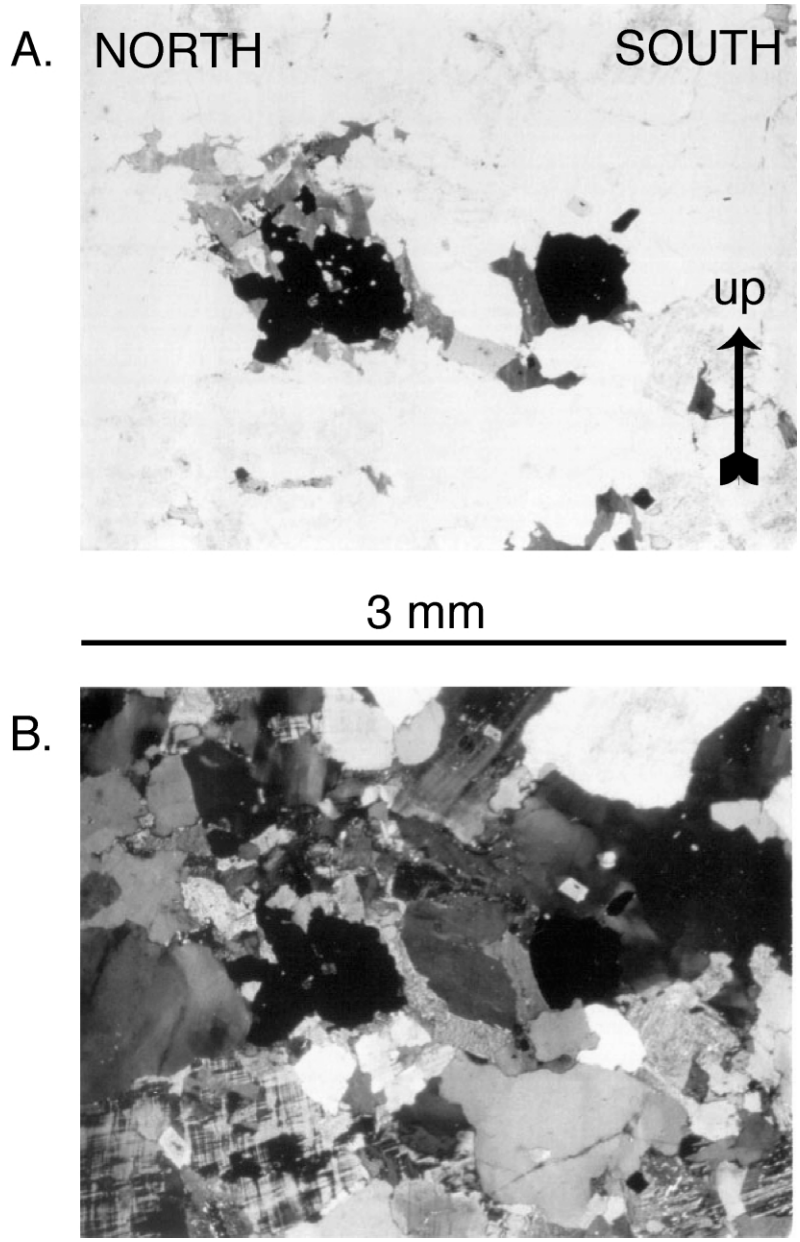

Fig. 3. A photomicrograph of the Mount Waldo pluton from core 32c2. It is a medium-grained, porphyritic granite containing potassium feldspar, quartz, plagioclase feldspar, and biotite. (A) Plane light. Large (magnetically multidomain) magnetite grains are intergrown with biotite. (B) Polarized light. Both quartz and feldspar grains are unaffected by solid state deformation.

layering. He mapped the foliation as everywhere steep or vertical, striking north–south in the interior of the pluton, but striking east–west parallel to the pluton's contact with its wall rock, within 2 km of the northern margin of the pluton. Trefethen (1944) observed no lineation association with the foliation. Wones (1991) shows no lineation or foliation in the granite, but Lux et al. (2000) and Lux and Good (2001) observed the foliation. They noted that neither crystallographic preferred orientation of quartz nor fracturing and faulting of feldspar crystals occurs. Based on this lack of petrographic evidence for solid state deformation of the granite, they argued that the foliation is entirely magmatic in origin. The significance of the orientation of the foliation is enigmatic.

Enclaves, the second feature, range in composition from felsic to mafic and are generally finer-grained than the granite (Lux and Gibson, 2000; Gibson et al., 2001). Their longest axis ranges from a few centimeters to a few meters long. Grain size ranges from fine- to medium-grained, and potassium feldspar phenocrysts occur in some enclaves. Gibson et al. (2001) reported that enclave compositions are typical less evolved in composition than the granite, but that major and trace elements show continuous trends from the least evolved enclave to the granite. They interpreted this

Fig. 4. Photograph of the Mount Waldo granite on a glacially polished surface. 2 lb crack hammer for scale. Potassium feldspar phenocrysts are the aligned white tabular minerals. Foliation defined by these feldspars is magmatic in origin and ubiquitous in the pluton.

data to indicate that enclaves result from magma mixing and hybridization during crystallization of the pluton.

Mafic schlieren, the third feature, are also present in the pluton but not common (Trefethen, 1944; Lux and Gibson, 2000; Lux et al., 2000; Lux and Good, 2001). These schlieren are dark planar layers characterized by high concentrations of biotite ± hornblende (and euhedral accessory allanite, titanite, zircon, magnetite, and apatite). Bottom contacts of schlieren with granite layers are sharp, but upper boundaries grade into granite. Schlieren commonly parallel the foliation defined by potassium feldspar phenocrysts, and some schlieren have forms of channels and troughs. Lux et al. (2000) and Lux and Good (2001) ascribe the schlieren and compositional layering to pseudosedimentary processes related to the deposition of newly crystallized minerals and flow along the contact between liquid magma and crystal mush underneath.

2.2. Regional geologic and tectonic relations

The Mount Waldo pluton was emplaced in the middle to upper crust in the Late Devonian. Stewart et al. (1995) reported a U–Pb zircon age of 371 ± 2 Ma (analyzed by R.D. Tucker). The Mount Waldo Pluton is associated with a 2–3-km-wide contact aureole of andalusite-grade metamorphism (Lux et al., 2000), and an emplacement pressure of ≤3 kbar is based on the Al-in-hornblende geobarometer (Lux and Gibson, 2000). The shape of the pluton in map view is roughly circular (Fig. 2), and it crops out over an area of approximately 150 km^2. Inverted gravity data from the region show the pluton as steep-walled, tabular, and roughly 2–4 km deep with some parts of it locally much deeper (Sweeney, 1972, 1976).

The pluton cuts across the faults, fabrics, and metamorphic gradients into which it intrudes (Osberg et al., 1985). The pluton intruded three different pre-Devonian metasedimentary units: the sillimanite-bearing Passagassawakeag Gneiss; the chlorite-bearing Bucksport Formation; and the Penobscot Formation (Fig. 2) (Osberg et al., 1985; Wones, 1991). The Sennebec Pond Fault and the Liberty–Orrington faults juxtapose these metamorphic units and are also cut by the Mount Waldo pluton. Because faunal successions on either side of the Sennebec Pond fault are distinct, Stewart et al. (1995) argued that this fault may have been a Silurian suture zone. A recent study by Short (2000) argued that the Liberty–Orrington Fault was a terrane boundary and an orogen-scale dextral shear zone during the Devonian. Wall rock units have subvertical northeast-striking foliation and subhorizontal northeast-trending lineation (Wones, 1991), both of which probably formed during Devonian dextral shearing. Wall rock foliation and lineation bend downward, parallel to the contact with the pluton at its eastern and southern margins (Wones, 1991). The mechanism by which the pluton was emplaced is unclear: mesoscale structures within the pluton are consistent with a dynamic magma chamber, and contact relations are consistent with forceful emplacement or late ballooning and sinking of the chamber.

The intrusion of the pluton probably coincided with dextral movement on the adjacent northeast-trending Norumbega Fault Zone (Figs. 1 and 2) (Wones, 1991; West and Hubbard, 1997; Ludman and West, 1999; West, 1999). Differing lines of evidence have suggested that Paleozoic dextral offset along the Norumbega fault ranges from a few tens of kilometers (estimated from offset metamorphic isograds by Robinson et al. (1998)) to 150 km (estimated from finite shear strains measured in the Casco Bay area by Swanson (1992)). West and Hubbard (1997) offered a solution to these diverse estimates with their four-dimensional model of late Devonian to Early Carboniferous deformation along the Norumbega Fault Zone. Progressive deformation and exhumation resulting from transpression

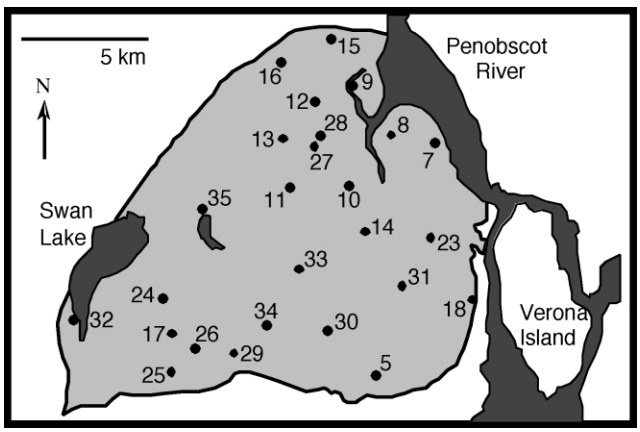

Fig. 5. Sample locations and site numbers in the Mount Waldo pluton. UTM coordinates for each site are in Table 1.

along the fault involved juxtaposition of various brittle and ductile structural styles that represent activity at different depths. West (1999) summarized a decade of research dating deformation fabrics and mineral cooling histories of rocks in the fault and its borderlands. Both West and Hubbard (1997) and West (1999) tentatively interpreted these data to suggest that activity along the Norumbega Fault Zone occurred continuously over a 100 m.y. period (from ~380 Ma—the Middle or Late Devonian—to ~280 Ma—the Late Carboniferous or Early Permian). If this chronology is correct, then the Norumbega fault was active during emplacement of the Mount Waldo pluton.

Table 1
UTM locations of sites

Site	Latitude UTM	Longitude UTM
5	511.51	4927.71
7	513.24	4937.07
8	511.72	4937.24
9	510.05	4939.17
10	510.02	4935.46
11	507.92	4935.39
12	508.92	4938.55
13	507.84	4936.67
14	510.63	4933.75
15	509.43	4930.41
16	507.58	4939.80
17	503.48	4929.60
18	514.72	4931.17
23	513.19	4933.70
24	503.24	4931.84
25	503.51	4928.41
26	504.24	4929.46
27	509.12	4937.36
28	509.17	4937.27
29	505.87	4929.10
30	509.22	4929.96
31	512.17	4921.43
32	499.75	4930.96
33	507.96	4932.31
34	506.75	4930.19
35	504.75	4934.07

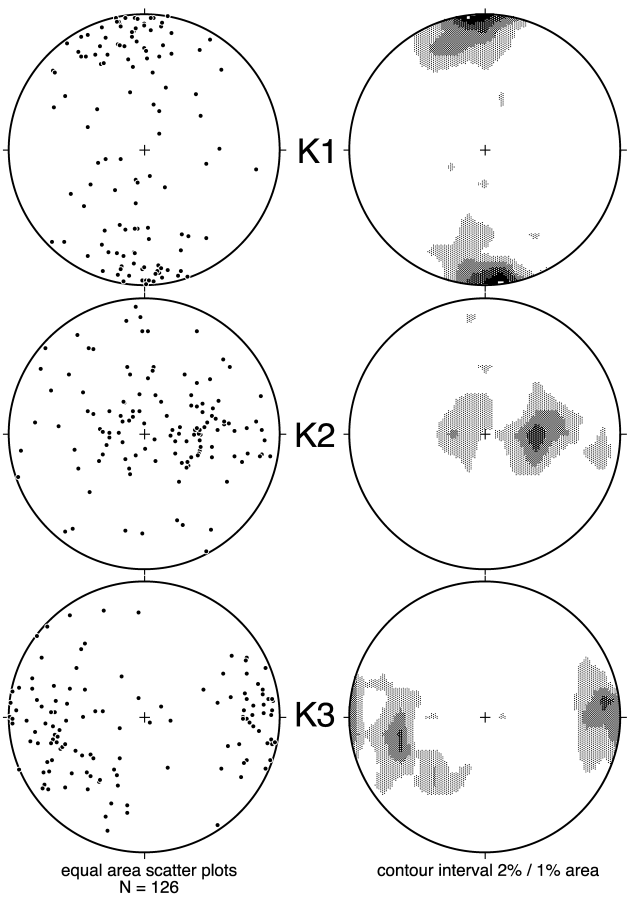

Fig. 6. Raw AMS data from each core in the study, from Table 2. The maximum susceptibility axes ($K1$, or AMS lineation) are generally subhorizontal, trending north–south. The minimum susceptibility axes ($K3$, or poles to AMS foliation) are also generally subhorizontal, but trending east–west.

3. Field and laboratory methods

One data set we gathered from the Mount Waldo pluton is field measurements of foliation defined by the preferred orientation of potassium feldspar phenocrysts. Outcrop in the study area is generally poor, and most exposures are small glacial pavement surfaces. At most of the 26 sites throughout the pluton (Fig. 5; Table 1), we measured the trend of feldspar foliation on glacial pavement. At three of these sites where outcrop was better (one quarry and two road cuts), we measured the strike and dip of this foliation.

The other data set is laboratory measurements of the anisotropy of magnetic susceptibility (AMS) of oriented cores. Magnetic susceptibility (K) measures the magnetization of a rock in an applied external magnetic field (Borradaile, 1988; Tarling and Hrouda, 1993; Bouchez, 1997). A second rank tensor describes the three-dimensional anisotropy of the magnetic susceptibility of rocks. Geometrically, (K) is a triaxial ellipsoid with a maximum, intermediate, and minimum axis: $K1$, $K2$ and $K3$, respectively. We measured each core (from four to six per site) using a SI2B Sapphire Magnetic Susceptibility and

Table 2
AMS data from each core

Site and core	$K1_{dec}$ (°)	$K1_{inc}$ (°)	$K1$ ($\times 10^{-6}$ SI)	$K2_{dec}$ (°)	$K2_{inc}$ (°)	$K2$ ($\times 10^{-6}$ SI)	$K3_{dec}$ (°)	$K3_{inc}$ (°)	$K3$ ($\times 10^{-6}$ SI)	K_{mean} ($\times 10^{-6}$ SI)	L ($K1/K2$)	F ($K2/K3$)	P ($K1/K3$)	T (shape) (°)	P' (°)
5A	186	25	96	304	45	92	77	35	89	92	1.047	1.036	1.084	−0.127	1.085
5D	103	51	108	351	17	104	249	34	100	104	1.032	1.045	1.078	0.172	1.078
5E	173	9	96	310	78	92	82	8	87	92	1.037	1.057	1.096	0.213	1.097
5E2	44	19	125	216	71	122	313	2	119	122	1.024	1.023	1.047	−0.024	1.047
7A	13	13	5113	128	61	5097	276	25	4785	4999	1.003	1.065	1.069	0.905	1.078
7B	349	6	5465	89	58	5232	256	31	5068	5255	1.045	1.032	1.078	−0.156	1.079
7C	352	2	7386	84	53	7035	261	37	6635	7019	1.050	1.060	1.113	0.093	1.113
7D	8	6	6869	107	55	6607	273	35	6223	6566	1.040	1.062	1.104	0.214	1.105
7D2	10	23	7071	203	67	6615	102	4	6195	6627	1.069	1.068	1.141	−0.009	1.141
7E	172	6	8093	75	47	7787	267	42	7454	7778	1.039	1.045	1.086	0.062	1.086
8A	356	11	8747	244	62	8291	91	25	7782	8273	1.055	1.065	1.124	0.085	1.124
8B	349	8	9151	91	56	8436	254	33	7644	8410	1.085	1.104	1.197	0.096	1.198
8C	354	17	12963	110	55	11749	254	29	11593	12102	1.103	1.013	1.118	−0.761	1.130
8C2	355	13	11129	202	76	10198	87	6	9911	10413	1.091	1.029	1.123	−0.508	1.128
8D	356	3	9096	90	57	8527	264	33	8210	8611	1.067	1.039	1.108	−0.261	1.109
9A	295	27	10394	86	59	9886	198	13	9785	10022	1.051	1.010	1.062	−0.661	1.067
9B	311	12	15234	50	37	14871	205	51	14338	14814	1.024	1.037	1.062	0.203	1.063
9C	346	54	7857	93	12	7600	191	34	7367	7608	1.034	1.032	1.067	−0.030	1.067
9D	333	30	6663	126	57	6481	236	12	6374	6506	1.028	1.017	1.045	−0.248	1.046
10A	4	3	5899	118	83	5483	273	6	5025	5469	1.076	1.091	1.174	0.089	1.174
10B	191	13	6601	349	76	5857	100	5	5773	6077	1.127	1.015	1.143	−0.784	1.158
10C	181	3	5406	86	56	4976	273	34	4767	5050	1.086	1.044	1.134	−0.317	1.136
10C2	3	13	4438	116	58	4233	266	28	3998	4223	1.048	1.059	1.110	0.093	1.110
10C3	187	7	5320	80	68	4961	279	21	4618	4967	1.072	1.074	1.152	0.013	1.152
11A	43	77	7635	217	13	7254	307	1	7002	7297	1.052	1.036	1.090	−0.183	1.091
11B	337	18	5400	157	72	5204	247	0	5149	5251	1.038	1.011	1.049	−0.550	1.051
11C	176	3	5647	83	37	5314	270	53	5133	5365	1.063	1.035	1.100	−0.272	1.102
11D	181	4	7553	84	58	7157	273	32	7021	7244	1.055	1.019	1.076	−0.473	1.079
11F	59	50	4535	295	25	4393	190	29	4138	4355	1.032	1.062	1.096	0.303	1.097
12A	324	3	10389	59	57	10122	232	33	9335	9948	1.026	1.084	1.113	0.514	1.118
12A2	346	21	8814	84	18	8528	211	61	8056	8466	1.034	1.059	1.094	0.267	1.095
12B	350	33	9250	104	32	9001	226	41	8650	8967	1.028	1.041	1.069	0.186	1.070
12C	335	30	8940	88	34	8739	215	41	8569	8749	1.023	1.020	1.043	−0.072	1.043
12D	331	5	21458	66	40	20217	235	50	19795	20490	1.061	1.021	1.084	−0.477	1.087
13A	173	15	5052	275	37	5010	65	50	4686	4916	1.008	1.069	1.078	0.779	1.086
13A	348	1	5128	257	46	4877	79	44	4760	4922	1.051	1.025	1.077	−0.347	1.079
13A2	356	21	3012	109	46	2855	250	36	2755	2874	1.055	1.036	1.093	−0.202	1.094
13B	333	22	4753	83	40	4382	222	41	4330	4488	1.085	1.012	1.098	−0.741	1.107
13C	334	6	7211	70	45	6727	238	45	6563	6834	1.072	1.025	1.099	−0.474	1.103
13C2	328	20	4039	122	68	3896	235	9	3769	3901	1.036	1.034	1.072	−0.038	1.072
14A	349	4	12937	94	74	12520	258	15	12021	12492	1.033	1.042	1.076	0.108	1.076
14A	179	4	10556	87	25	10013	278	65	9624	10064	1.054	1.040	1.097	−0.142	1.097

(*continued on next page*)

Table 2 (*continued*)

Site and core	$K1_{dec}$ (°)	$K1_{inc}$ (°)	$K1$ ($\times 10^{-6}$ SI)	$K2_{dec}$ (°)	$K2_{inc}$ (°)	$K2$ ($\times 10^{-6}$ SI)	$K3_{dec}$ (°)	$K3_{inc}$ (°)	$K3$ ($\times 10^{-6}$ SI)	K_{mean} ($\times 10^{-6}$ SI)	L ($K1/K2$)	F ($K2/K3$)	P ($K1/K3$)	T (shape) (°)	P' (°)
14B	204	24	8240	16	66	7972	113	3	7846	8019	1.034	1.016	1.050	−0.352	1.051
14C	360	26	6729	242	44	6604	109	35	6393	6575	1.019	1.033	1.053	0.265	1.053
14D	254	61	8322	356	7	8204	90	28	7841	8122	1.014	1.046	1.061	0.523	1.064
15A	239	37	12527	51	53	11819	146	4	11449	11932	1.060	1.032	1.094	−0.294	1.096
15b	152	64	10082	262	9	9985	357	24	9480	9849	1.010	1.053	1.064	0.685	1.069
15c	21	65	10943	145	15	10706	240	20	10482	10710	1.022	1.021	1.044	−0.019	1.044
15c2	89	44	7892	329	28	7538	218	33	7391	7607	1.047	1.020	1.068	−0.399	1.070
16A	43	43	6818	302	11	6740	201	45	6415	6658	1.012	1.051	1.063	0.622	1.067
16B	311	14	9262	219	8	8933	98	74	8846	9014	1.037	1.010	1.047	−0.572	1.050
16C	304	30	8120	80	51	7939	201	22	7439	7833	1.023	1.067	1.092	0.484	1.095
16D	100	17	5574	347	53	5493	201	32	5091	5386	1.015	1.079	1.095	0.677	1.102
17a	0	8	7194	253	66	6913	93	23	6338	6815	1.041	1.091	1.135	0.371	1.138
17b	192	6	9364	82	73	8901	284	16	8318	8861	1.052	1.070	1.126	0.143	1.126
17C	3	3	6265	264	69	6017	95	20	5486	5923	1.041	1.097	1.142	0.392	1.146
17d	178	4	4663	276	63	4530	86	27	4363	4519	1.029	1.038	1.069	0.130	1.069
18A	225	4	177	129	57	165	317	32	161	168	1.076	1.022	1.099	−0.546	1.104
18b	256	66	164	27	16	160	122	17	154	159	1.029	1.038	1.068	0.131	1.068
18c	169	10	236	299	75	152	77	11	96	161	1.554	1.593	2.474	0.027	2.511
18d	198	41	6	46	45	4	300	14	2	4	1.778	2.118	3.765	0.132	3.943
23a	174	11	8901	327	78	8449	83	5	8127	8493	1.053	1.040	1.095	−0.145	1.096
23b	221	11	10870	311	4	10439	60	78	10041	10450	1.041	1.040	1.083	−0.020	1.083
23c	10	0	7840	101	48	7477	280	42	7289	7535	1.049	1.026	1.076	−0.300	1.077
23d	16	27	9363	276	20	8540	155	56	8117	8673	1.096	1.052	1.154	−0.288	1.156
24A	199	21	72	87	45	68	306	38	65	68	1.050	1.054	1.106	0.040	1.107
24B	341	14	996	100	64	944	245	22	910	950	1.055	1.038	1.095	−0.175	1.095
24C	216	60	64	359	25	62	97	16	62	63	1.029	1.008	1.037	−0.559	1.039
24C2	31	6	64	291	57	63	124	32	58	61	1.021	1.085	1.107	0.597	1.114
24D	181	13	396	333	75	382	89	7	375	384	1.037	1.017	1.055	−0.377	1.056
24E	208	12	64	328	68	61	113	19	60	62	1.059	1.013	1.073	−0.626	1.078
25A	160	22	6073	327	67	5901	68	4	5256	5743	1.029	1.123	1.155	0.604	1.165
25B	349	23	14480	199	64	14302	84	12	13105	13962	1.012	1.091	1.105	0.751	1.115
25C	177	42	8272	346	48	8116	82	5	7355	7914	1.019	1.104	1.125	0.677	1.134
25E	172	13	11863	307	72	11452	79	12	10492	11269	1.036	1.092	1.131	0.426	1.135
26A	0	9	9200	175	81	8769	270	1	8126	8698	1.049	1.079	1.132	0.227	1.134
26C	172	5	6043	273	65	5701	80	24	5386	5710	1.060	1.058	1.122	−0.012	1.122
26D	167	74	3604	358	15	3510	267	3	3433	3515	1.027	1.023	1.050	−0.084	1.050
26E	165	4	12820	273	75	11926	74	14	11400	12049	1.075	1.046	1.125	−0.231	1.126
26F	180	14	8978	303	65	8455	84	20	7986	8473	1.062	1.059	1.124	−0.024	1.124
27A	347	22	8545	112	55	8259	245	26	7919	8241	1.035	1.043	1.079	0.106	1.079
27b	356	11	8699	103	55	8402	259	33	8003	8368	1.035	1.050	1.087	0.167	1.087
27c	339	26	10002	123	59	9354	241	16	8860	9405	1.069	1.056	1.129	−0.105	1.129
27c2	352	38	9783	101	23	9418	215	43	8967	9389	1.039	1.050	1.091	0.127	1.091
28A	163	7	6898	63	54	6460	257	35	5919	6426	1.068	1.091	1.165	0.143	1.166
28b	161	1	8599	70	52	8325	251	38	7969	8298	1.033	1.045	1.079	0.150	1.079

(*continued on next page*)

Table 2 (*continued*)

Site and core	$K1_{dec}$ (°)	$K1_{inc}$ (°)	$K1$ ($\times 10^{-6}$ SI)	$K2_{dec}$ (°)	$K2_{inc}$ (°)	$K2$ ($\times 10^{-6}$ SI)	$K3_{dec}$ (°)	$K3_{inc}$ (°)	$K3$ ($\times 10^{-6}$ SI)	K_{mean} ($\times 10^{-6}$ SI)	L ($K1/K2$)	F ($K2/K3$)	P ($K1/K3$)	T (shape) (°)	P' (°)
28C	19	50	6437	159	32	6237	262	20	5773	6149	1.032	1.080	1.115	0.419	1.119
28d2	175	9	7693	52	73	7120	268	14	6833	7215	1.080	1.042	1.126	−0.306	1.128
29A	177	34	9273	4	56	9040	269	3	8289	8867	1.026	1.091	1.119	0.546	1.125
29B	185	41	7634	8	49	7363	276	1	6932	7309	1.037	1.062	1.101	0.251	1.102
29C	6	42	8882	223	41	8437	115	20	7875	8398	1.053	1.071	1.128	0.146	1.128
29D1	193	39	7750	8	51	7559	101	2	6835	7381	1.025	1.106	1.134	0.603	1.142
29D2	199	6	6230	2	84	6021	109	2	5650	5967	1.035	1.066	1.103	0.303	1.104
30A1	292	53	5393	157	28	5330	55	22	5144	5289	1.012	1.036	1.048	0.507	1.050
30A2	187	41	5427	308	30	5125	61	34	5056	5203	1.059	1.014	1.073	−0.617	1.078
30B	196	71	10420	326	13	9523	60	14	8984	9642	1.094	1.060	1.160	−0.214	1.161
30C	248	75	1957	152	2	1930	61	15	1851	1913	1.014	1.043	1.057	0.501	1.060
30d	237	51	5113	2	25	4898	106	28	4843	4951	1.044	1.011	1.056	−0.584	1.059
31A	187	41	8558	34	46	8288	289	14	8108	8318	1.033	1.022	1.056	−0.185	1.056
31B	185	24	7855	88	14	7611	331	62	7358	7608	1.032	1.034	1.068	0.036	1.068
31d1	195	22	14850	353	66	13934	102	8	13573	14119	1.066	1.027	1.094	−0.417	1.097
30d2	185	17	10453	78	45	9912	291	41	9788	10051	1.055	1.013	1.068	−0.618	1.072
32a	348	4	288	90	69	268	256	20	262	273	1.073	1.026	1.101	−0.458	1.105
32b	9	31	9484	120	30	8923	244	43	8453	8953	1.063	1.056	1.122	−0.060	1.122
32b2	1	28	5339	106	26	5147	231	50	4987	5158	1.037	1.032	1.070	−0.078	1.071
32C	357	4	11335	249	76	10379	88	13	9832	10515	1.092	1.056	1.153	−0.238	1.155
32C	179	1	11287	271	69	10491	89	21	10011	10596	1.076	1.048	1.127	−0.219	1.129
32C2	354	14	12226	239	58	11163	91	28	10641	11343	1.095	1.049	1.149	−0.311	1.152
33A	189	57	12761	327	26	12529	67	19	12274	12521	1.018	1.021	1.040	0.058	1.040
33B	191	21	1403	28	68	1355	283	6	1205	1321	1.035	1.124	1.164	0.541	1.173
33b2	189	2	1099	97	56	1035	280	34	1011	1048	1.062	1.024	1.087	−0.431	1.090
33C1	156	32	4316	52	21	4150	295	50	3950	4138	1.040	1.051	1.093	0.115	1.093
33C2	145	21	3574	47	21	3403	276	60	3311	3429	1.050	1.028	1.079	−0.287	1.081
34A	29	17	5458	144	54	5317	289	30	5236	5337	1.026	1.015	1.042	−0.259	1.043
34b	192	70	3334	72	10	3281	339	17	3231	3282	1.016	1.015	1.032	−0.026	1.032
34C	227	39	7510	63	50	7317	324	8	7295	7374	1.027	1.003	1.030	−0.794	1.033
34d1	12	62	3126	191	28	3086	281	1	3040	3084	1.013	1.015	1.028	0.060	1.028
34d2	206	34	4242	81	40	4227	321	31	4159	4209	1.004	1.016	1.020	0.636	1.021
35A	191	11	221	100	6	208	343	78	206	212	1.060	1.012	1.072	−0.666	1.077
35b	311	52	1244	181	27	1177	77	25	1116	1179	1.057	1.055	1.115	−0.016	1.115
35C	2	33	1303	101	14	1258	210	53	1194	1252	1.035	1.054	1.091	0.200	1.091
35d1	153	29	214	292	53	200	51	20	197	204	1.073	1.015	1.089	-0.657	1.095

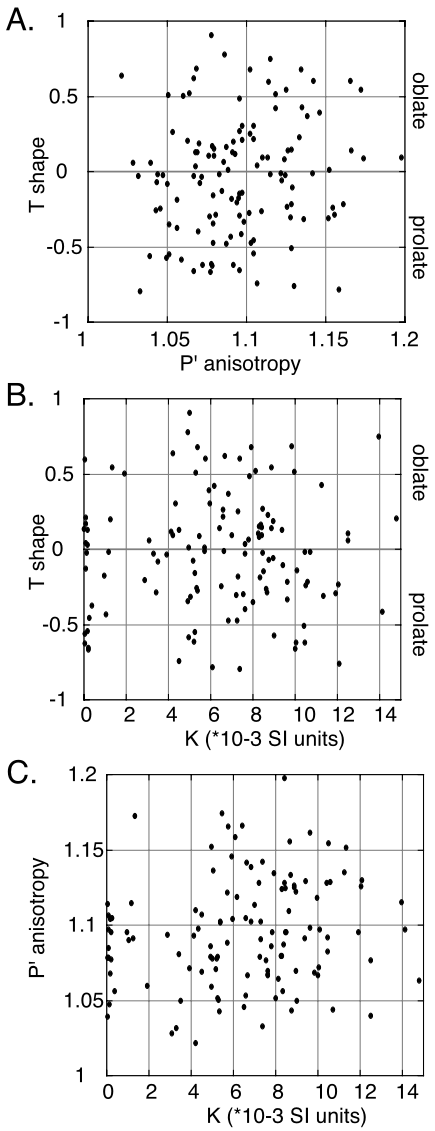

Fig. 7. Jelinek (1981) plots of raw AMS data from each core. (A) A plot of anisotropy vs. shape of the AMS ellipsoid from each core shows relatively low anisotropy and no preference for oblate or prolate ellipsoids. (B) A plot of bulk susceptibility vs. anisotropy shows no relation between the two, consistent with a single magnetic mineralogy responsible for AMS signal. (C) A plot of bulk susceptibility vs. anisotropy. Relatively high bulk susceptibilities of samples are consistent with magnetite control of AMS signal.

Anisotropy Meter (Stupavsky, 1984; Borradaile and Stupavsky, 1995) at Mount Holyoke College. The meter measures each core 12 times in six different orientations using a field of 13,000 Gauss at a frequency of 750 Hz. The SI2B program returns $K1$, $K2$, and $K3$ for each core. Based on these data, we calculated several other common parameters to characterize the susceptibility ellipsoid of samples in this study: lineation magnitude of the ellipsoid (L, how prolate the ellipsoid is), foliation magnitude of the ellipsoid (F, how oblate the ellipsoid is), Jelinek's (1981) shape parameter T (when T is negative, the shape is more prolate, and when T is positive, the shape is more oblate), total anisotropy of the susceptibility ellipsoid (P), and another measure of the total anisotropy (P', from Jelinek, 1981). The same software that runs the SI2B Meter averages core data to return $K1$, $K2$, and $K3$ at each site.

For some cores, we also present the results of acquired isothermal remanent magnetization experiments in fields up to 1.25 Tesla. We acquired these data with an ASC Scientific model IM-10 impulse magnetometer and a spinner magnetometer at the University of Massachusetts.

4. Results

The orientations, but not shapes, of the AMS ellipsoid are consistent among most cores (Fig. 6; Table 2). In general, the longest axes of the susceptibility ellipsoid ($K1$) trend N–S and are sub-horizontal. The intermediate axes of the susceptibility ellipsoid ($K2$) are generally subvertical, and the minimum axes ($K3$) subhorizontal, trending E–W. About half the cores have a susceptibility ellipsoid that is oblate, and the other half prolate (Fig. 7a; Table 2). Anisotropy (P') is generally less than 1.15, and the shape (T) and anisotropy (P') of AMS ellipsoids appear unrelated (Fig. 7a).

High bulk susceptibility (K) in most cores (Fig. 7b and c; Table 2) suggests that the ferromagnetic mineral magnetite controls the AMS in these samples (Rochette, 1987). Rochette et al. (1992) argued that a correlation between bulk susceptibility and anisotropy suggests that varying amounts of different magnetic minerals may be responsible for variations in the shape of the AMS ellipsoid. In our samples, however, both the shape and anisotropy of the AMS ellipsoid are unrelated to the bulk susceptibility (Fig. 7b and c). The data presented in Fig. 7c therefore further suggest that magnetite alone controls the shape and anisotropy of AMS of most cores.

The results of acquired isothermal remanent magnetization (IRM) experiments are also consistent with magnetite control of rock magnetic properties (Fig. 8). Four samples (27a, 28d2, 32a, and 32c) reached full magnetization at relatively low applied voltages, a behavior characteristic of magnetite (Dunlop, 1972). One sample (5e) never acquired an IRM and appears not to contain magnetite. None of the samples shows evidence for hematite. These results are consistent with petrographic observations and AMS results.

The agreement between AMS foliation data and field data on feldspar foliation is excellent. For the AMS data, $K3$ represents the pole to AMS foliation, and this foliation is subvertical and strikes north–south for most cores (Fig. 6). The traces of feldspar foliation measured on sub-horizontal glacial pavement exposures also show a strong preferred orientation and trend north–south (Fig. 9). At three different three-dimensional exposures, this feldspar foliation is variable, but also generally subvertical and striking north–south (Fig. 10). At two of these exposures (sites 28 and 32), the foliations defined by feldspars and AMS are subparallel

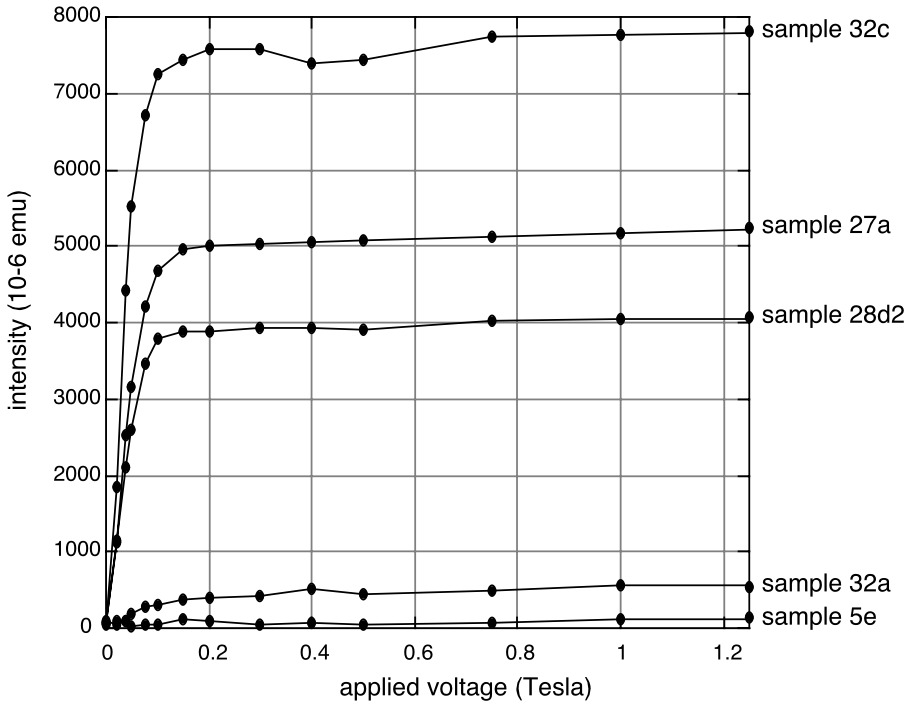

Fig. 8. Results of progressive isothermal remanent magnetization (IRM) experiments on five cores. These data (with the exception of sample 5e) are consistent with the occurrence of magnetite rather than hematite.

(Fig. 10b and c). In the cases of these two sites and many others, consistent AMS results correlate to high susceptibilities and the presence of magnetite. At another exposure (site 5), the orientations of the principal axes of the susceptibility ellipsoids from each core do not agree with each other or with the foliation defined by feldspars (Fig. 10a). Although each core at this site displays a magnetic foliation and lineation, the site itself does not show a consistent fabric. We observe similar data in sites on both the northern and southern edge of the pluton and at some other sites. In the case of this site and some others, internally inconsistent AMS results correlate to low susceptibilities and the absence of magnetite.

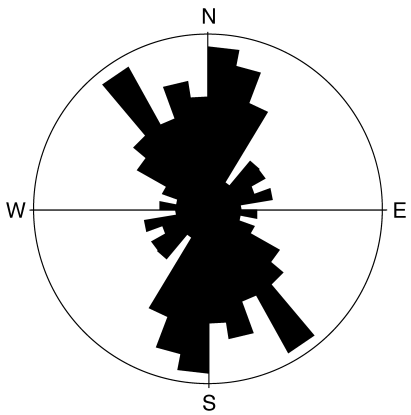

Fig. 9. Rose diagram showing orientation of feldspar fabric measured on glacial pavement surfaces at most sites. $N = 95$, circle = 11%. Feldspars define a strong fabric that trends north–south on these subhorizontal surfaces.

The AMS data also reveal a previously unrecognized lineation. The AMS lineation is the longest axis of the susceptibility ellipsoid ($K1$). In most cores, the AMS lineation trends north–south and is sub-horizontal (Figs. 6 and 10b and c).

At most sites, the orientations of the principal axes of the susceptibility ellipsoids from each core agree with each other and show a subvertical, north–south-striking foliation and a horizontal, north–south-trending lineation (Table 3; Figs. 11 and 12). For 18 of the 26 sites (including sites 28 and 32 discussed above), we present data on the site-averaged orientation of the AMS ellipsoid. In other cases (such as that of site 5 discussed above), we report a mean susceptibility but no data pertaining to the orientation of the AMS ellipsoid. Lineation trends north–northwest in the northeast corner of the pluton, and south–southwest in the southern half of the pluton (Fig. 11). The plunge varies but is generally sub-horizontal across the pluton. Foliation throughout the pluton strikes roughly north–south (Fig. 12). In the northeast and southwest corner of the pluton, its strike is more north–northwest. In the southeast corner, its strike is more north–northeast. The dips of foliation in the east side of the pluton are toward the east, more steeply along the edge and less steeply towards the center. The dips of the foliation in the west side of the pluton are toward the west, dipping more steeply along the edge and less steeply towards the center. Foliation is generally steep to subvertical.

Many sites show large variations between cores in the shape (T) of the fabric ellipsoids (Table 3). Some generally

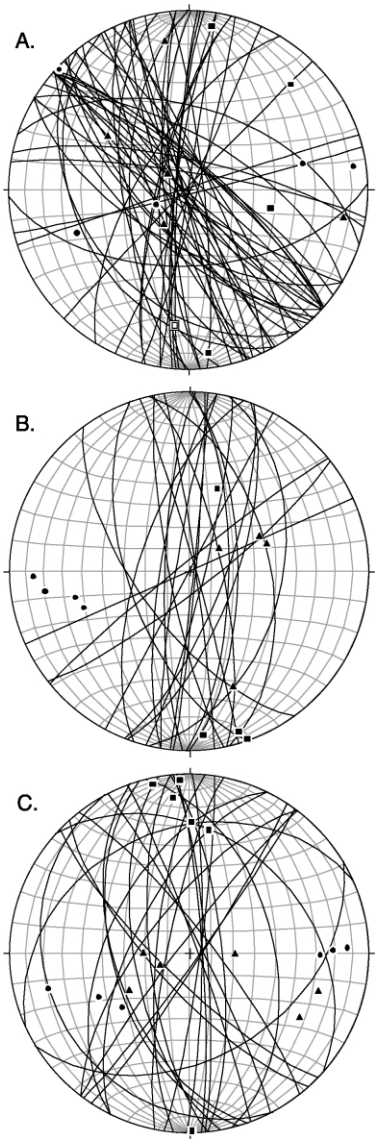

Fig. 10. Equal area stereographic projections of raw AMS and field data from the study. Great circles represent feldspar foliations that we measured in the field (see Fig. 4 for an example). Symbols represent AMS data measured on oriented cores. Squares are $K1$, triangles are $K2$, and circles are $K3$. (A) Data from site 5. Although feldspar fabric is well defined, AMS fabric is not. (B) Data from site 28. Feldspar and AMS fabrics are well defined and agree with each other. (C) Data from site 32. Again, feldspar and AMS fabrics are well defined and agree with each other.

show oblate AMS ellipsoids (such as at site 28), and others generally show prolate ellipsoids (such as at site 32).

5. Discussion

5.1. Significance of magnetic fabric in the pluton

Petrographic observations (Fig. 3), AMS results (Table 2; Fig. 7), and IRM results (Fig. 8) strongly suggest that the predominant magnetic mineral in the Mount Waldo pluton is magnetite. Petrologic study further shows the magnetite grains are large (up to 500 μm), suggesting that the magnetite is multi-domain. Although the mineral composition and grain size of a rock determine the strength and nature of the rock's magnetic susceptibility, ferromagnetic minerals (i.e. magnetite) have a susceptibility one to two magnitudes stronger than the others (Tarling and Hrouda, 1993). Thus in rocks containing magnetite, it controls the magnetic susceptibility of the rock (Bouchez, 1997).

Although AMS has become a standard semi-quantitative tool for the mapping of granite fabrics (Bouchez, 1997), some controversy exists as to its significance. The significance of AMS, when carried by multi-domain magnetite (such as is the case in the Mount Waldo pluton), may relate to any of three factors: (1) shape-preferred orientation of longest axes of magnetite grains (Uyeda et al., 1963); (2) distribution anisotropy of magnetite grains (Hargraves, 1991); or (3) preferred orientation of domain walls within magnetite grains (Borradaile and Kehlenbeck, 1996).

Shape-preferred orientation of magnetite grains, the first of these explanations, adequately explains the AMS data presented here. Magnetite is generally intergrown with biotite, and magnetite grains are commonly longer in one dimension than others (as in the magnetite grain on the left in Fig. 3a). Although magnetite is a crystallographically isometric phase, it often shows such morphological anisotropy. The susceptibility is strongest when the applied magnetic field is parallel to the longest axes of these multi-domain magnetite crystals. When the direction of the applied magnetic field is perpendicular to the longest axes of these crystals, the susceptibility is weaker. Because magnetite grains in the Mount Waldo pluton generally have their longest axes oriented sub-horizontal, trending north–south, this shape-preferred orientation of magnetite grains may explain the magnetic foliation and lineation.

Neighboring magnetite grains, however, are commonly close enough (as in Fig. 3a) to merit consideration of a distribution anisotropy, the second interpretation above. Hargraves et al. (1991) argued that when the AMS signal is produced by large (multi-domain) magnetite grains, the interpretation of AMS fabric is hampered by: (1) magnetite grains that are typically equant or skeletal, and (2) magnetite that has crystallized interstitially after magma flow has ceased (and should not define the same flow fabric as other phases). Their experiments suggested that magnetite growth follows a template established by the preferred orientation of silicates and that the anisotropic magnetic interaction between the magnetite grains is the generator of the AMS. They termed this phenomenon 'distribution anisotropy'. Such distribution anisotropy may also account for some of the AMS signal of this granite.

Because both of the first two interpretations appear to adequately explain AMS fabric in the Mount Waldo pluton, we do not further consider the third explanation above. This interpretation was introduced by Borradaile and Kehlenbeck (1996), who studied two related plutons in the Canadian

Table 3
AMS data from each site (averages of cores)

Site	No. cores	*K* avg. (E-6 SI)	St. dev. (E-6 SI)	Fabric ellipsoid	Lineation (*K*1)		Foliation (*K*3 pole)	
					Trend	Plunge	Strike	Rhand dip
5	4	102	14	Mixed	–	–	–	–
7	6	6374	1061	Mixed	356	7	354	72
8	5	9562	1663	Mixed	354	10	351	75
9	4	9738	3689	Prolate (3/4)	318	32	299	62
10	5	5157	683	Mixed	185	2	5	72
11	5	5902	1309	Prolate (4/5)	–	–	–	–
12	5	11,324	5154	Mixed	337	19	315	43
13	6	4656	1316	Mixed	342	10	335	58
14	5	9055	2287	Mixed	–	–	–	–
15	4	10,025	1824	Oblate (3/4)	–	–	–	–
16	4	7222	1557	Oblate (3/4)	–	–	–	–
17	4	6529	1819	Oblate (4/4)	0	0	181	75
18	4	123	80	Oblate (3/4)	–	–	–	–
23	4	8788	1216	Prolate (4/4)	–	–	–	–
24	6	265	359	Mixed	195	13	194	88
25	4	9722	3627	Oblate (4/4)	168	16	166	81
26	5	7689	3239	Prolate (4/5)	174	10	172	76
27	4	8851	633	Oblate (3/4)	349	25	332	59
28	4	7022	963	Oblate (3/4)	350	3	348	62
29	5	7585	1123	Oblate (4/5)	189	25	187	87
30	5	5400	2757	Mixed	230	65	156	66
31	4	10,024	2917	Prolate (3/4)	188	26	22	62
32	6	7806	4306	Prolate (6/6)	358	14	357	85
33	5	4492	4681	Mixed	173	28	11	60
34	5	4657	1761	Mixed	–	–	59	78
35	4	711	583	Mixed	–	–	–	–

shield. Although these plutons have no shape-preferred orientation or distribution anisotropy of magnetite or other magnetic phases, AMS foliation and lineation are well defined. They ascribed this AMS fabric to a late 'cryptic' tectonic overprint on the pluton, perhaps a stress field that was recorded only by magnetite domain walls. No further research has tested the feasibility or existence of this phenomenon.

The robust agreement between AMS and feldspar fabrics allows us to confidently use the AMS results as a measure of foliation and lineation in the pluton. At the two sites where good exposure and high magnetic susceptibility allow for a direct comparison between AMS and feldspar fabrics, the two foliations have the same orientation (Fig. 10b and c). Generally, both feldspar and AMS foliation are subvertical and strike north–south (Figs. 6, 9, 10 and 12). Lineation is only rarely visible in the field, a common problem in the study of granite fabrics. Nonetheless, the AMS lineation is

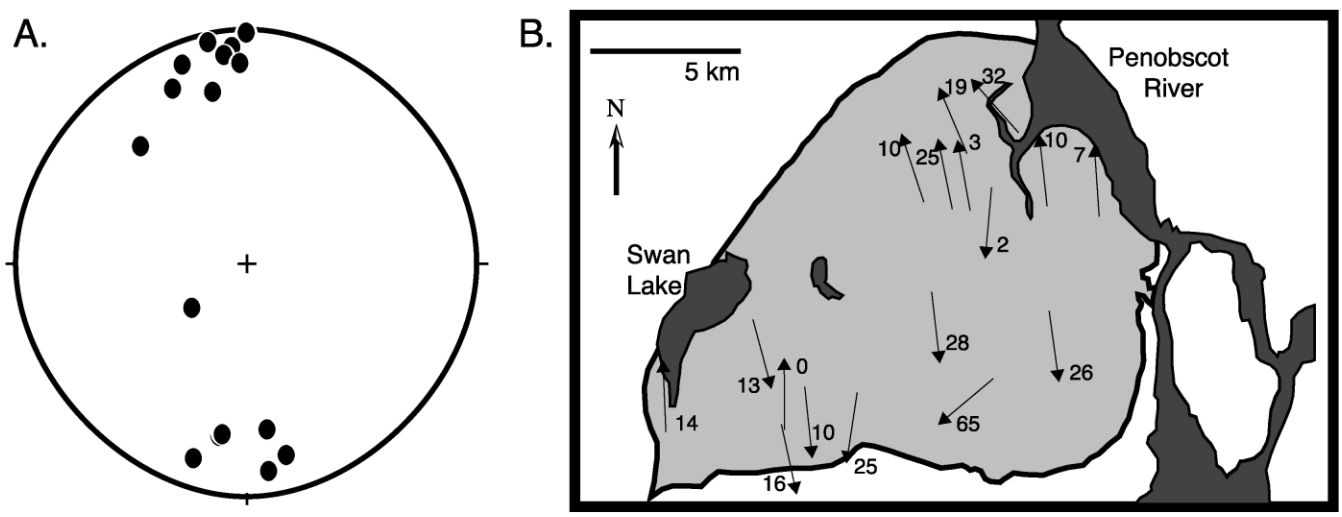

Fig. 11. (A) Equal area stereographic projection of magnetic lineation from sites listed in Table 3. (B) Map of same magnetic lineations in the pluton.

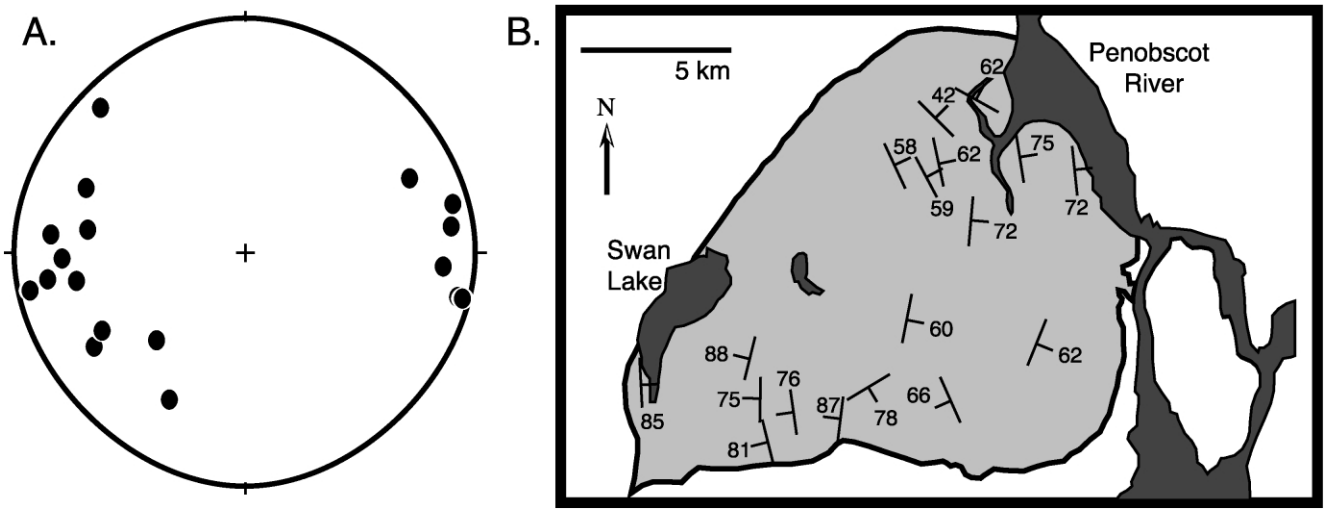

Fig. 12. (A) Equal area stereographic projection of poles to magnetic foliation from sites listed in Table 3. (B) Map of the same magnetic foliations in the pluton.

significant because it is so consistently oriented subhorizontal, trending north–south. Because the AMS fabrics are related to magnetite, and because magnetite is intergrown with biotite, the AMS foliation and lineation probably relate to the preferred orientation of biotite crystals. The shape- (and crystallographic-) preferred orientation of biotite and feldspar crystals agree well throughout the pluton (Trefethen, 1944; Lux and Gibson, 2000).

Both the foliation and lineation are magmatic in origin (Trefethen, 1944; Lux and Gibson, 2000). In thin section, both quartz and feldspar crystals lack evidence for internal deformation; neither crystallographic preferred orientation of quartz nor fracturing and faulting of feldspar crystals occurs (Fig. 3). Instead, the fabrics are associated with the shape preferred orientation of feldspar and biotite crystals. This observation suggests that the pluton acquired its magmatic fabric by the rigid rotation of biotite and feldspar crystals in response to magmatic flow in the pluton during crystallization. Rotation of biotite and feldspar crystals probably occurred soon after emplacement of the pluton, when it was in a partially molten state.

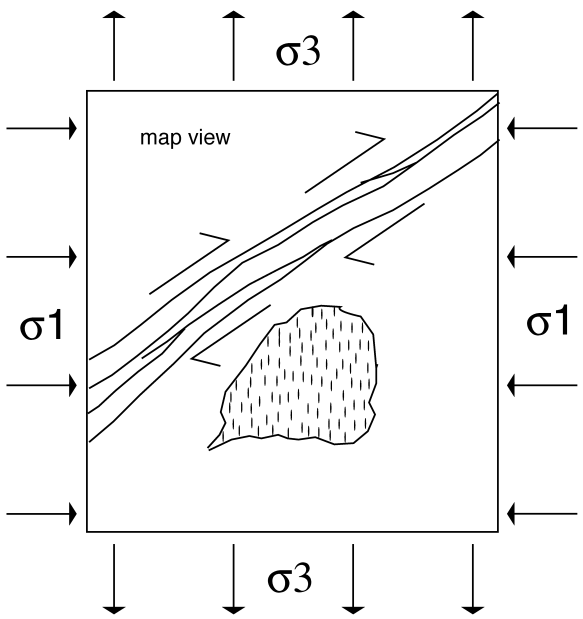

Fig. 13. Magmatic lineation and foliation formed in the Mount Waldo pluton during its Late Devonian crystallization in response to a small increment of regional crustal strain. From this small strain, we infer the late Devonian maximum principal stress ($\sigma 1$) as the pole to the pluton's foliation, and the minimum principal stress ($\sigma 3$) as parallel to the pluton's lineation. This crustal stress regime is consistent with concurrent dextral strike slip along the Norumbega Fault.

5.2. Significance of magmatic foliation and lineation

The complete lack of evidence for solid state deformation of the pluton strongly suggests that the pluton acquired its fabric in a short time-span, while crystallizing. Because the pluton is relatively small and intruded into the upper crust, it probably cooled and crystallized quickly with respect to crustal strain rates. Recent work on granite formation (summarized in Petford et al., 2000) suggests that pluton emplacement and cooling could have taken place in much less than one million years.

The orientation of magmatic foliation and lineation suggests that they developed in response to crustal-scale deformation rather than magma chamber processes such as convective flow or crystal settling on the chamber floor. Convective flow should generate fabric whose orientation varies locally in the chamber, and crystal settling should generate a subhorizontal fabric. Instead, foliation is subvertical and strikes north–south, and lineation is subhorizontal and trends north–south, regardless of location in the pluton. Previous AMS studies have generally interpreted similar patterns as tectonic in origin and related to the preservation of a large finite strain absorbed by the pluton in an igneous state (for example, Saint Blanquat and Tikoff, 1997).

We interpret the magmatic fabric as the record of a relatively small increment of crustal strain at the time of crystallization of the pluton (the Late Devonian). Evidence for Devonian to Carboniferous deformation related to the Norumbega Fault Zone suggests that the crust was experiencing regional deformation during the late Devonian crystallization of the pluton (West and Hubbard, 1997; West, 1999); however, the round shape of the pluton in map view indicates that the pluton did not experience a large strain. In addition, the amount of time for emplacement and crystallization of the pluton ($\ll$1 m.y.) is quite short compared with crustal strain rates. Because the pluton deformed during crystallization and not in the solid state, it must have acquired its fabric in a geologically brief time interval. Apparently, the pluton accommodated strain in its partially crystallized state because it was weak. After complete crystallization of the pluton, neighboring weak schists accommodated further crustal strain.

Because a small increment of strain records stress, magmatic foliation and lineation serve as a record of a Late Devonian stress field in the middle to upper crust (Fig. 13). We infer a Late Devonian maximum principal stress (σ1) oriented horizontal and east–west (perpendicular to the magmatic foliation in the pluton). We also infer a Late Devonian minimum principal horizontal stress (σ3) oriented horizontal and north–south (parallel to the magmatic lineation in the pluton). The intermediate principal stress (σ2) was vertical. In Anderson's (1951) traditional analysis, this crustal stress regime corresponds to strike-slip faulting. In fact, the orientation of Late Devonian principal stresses that we report here is consistent with dextral strike-slip movement on the Norumbega Fault, synchronous with crystallization of the Mount Waldo pluton (Fig. 13).

6. Conclusions

In the late Devonian Mount Waldo pluton, magmatic fabric is defined by both AMS data and the preferred orientation of biotite and feldspar crystals. The fabric formed during crystallization of the pluton, by rigid rotation of biotite and potassium feldspar crystals in a partially molten granitic mush. Throughout the pluton, foliation is subvertical and strikes north–south, and lineation is subhorizontal and trends north–south. Such consistent orientation of the fabric suggests that it formed in response to a small increment of crustal-scale strain. Such a strain is consistent with a dextral strike-slip stress regime during the Late Devonian in the Penobscot Bay region. This interpretation has a few interesting regional tectonic implications. First, it supports regional tectonic reconstructions that include continuous activity along the Norumbega fault from the Devonian to the Carboniferous (West and Hubbard, 1997). Second, it implies that the Mount Waldo pluton is either syntectonic or late tectonic in origin. Heretofore, most work had considered the pluton as post-tectonic because of its shape.

Acknowledgments

This work was funded by the Marland Pratt Billings and Katharine Fowler-Billings Fund for research in New England Geology, by Mount Holyoke College, and by the University of Massachusetts. Reviews by B. Clarke, Jim Evans, and an anonymous reviewer improved our writing. Thanks to Grace Bianciardi for coring with us and being cheerful; Mike Stupavsky and Mike Jackson for patience with questions about AMS and susceptibility meters; Dave Stewart and Dan Lux for sharing their knowledge of regional geology and geophysics; to Laurie Brown for access to her rock magnetic lab and her help; to Salma Monani for help with AMS; to Charlie Guidotti for providing an introduction to Maine geology; and to the many landowners in Waldo County who kindly let us drill holes in the ledge in their back yards.

References

Anderson, E.M., 1951. The Dynamics of Faulting and Dyke Formation with Applications to Britain, Oliver and Boyd, Edinburgh.

Balk, R., 1937. Structural Behavior of Igneous Rocks, Geological Society of America Memoir, New York.

Benn, K., Sawyer, E.W., Cruden, A.R., 1998. Preface to Special Issue on "Extraction, transport and emplacement of granitic magmas". Journal of Structural Geology 20, v–ix.

Borradaile, G.J., Kehlenbeck, M.M., 1996. Possible cryptic tectono-magnetic fabrics in 'post-tectonic' granitoid plutons of the Canadian Shield. Earth and Planetary Science Letters 137, 119–127.

Borradaile, G.J., Stupavsky, M., 1995. Anisotropy of magnetic susceptibility; measurement schemes. Geophysical Research Letters 22, 1957–1960.

Bouchez, J.L., 1997. Granite is never isotropic: an introduction to AMS studies of granitic rocks. In: Bouchez, J.L., Hutton, D.W.H., Stephens, W.E. (Eds.), Granite: from Segregation of Melt to Emplacement Fabrics. Kluwer, Dordrecht, The Netherlands, pp. 95–112.

Dunlop, D.J., 1972. Magnetic mineralogy of unheated and heated red sediments by coercivity spectrum analysis. Geophysical Journal of the Royal Astronomical Society 27, 37–55.

Gibson, D., Lux, D.R., Hogan, J.P., 2001. Geochemistry of enclaves and schlieren from the Mount Waldo Pluton, Maine; implications for magma chamber processes. Geological Society of America Northeast Section, Abstracts with Programs A-68, Vol. 33, No. 1.

Hargraves, R.B., Johnson, D., Chan, C.Y., 1991. Distribution anisotropy; the cause of AMS in igneous rocks? Geophysical Research Letters 18, 2193–2196.

Jelinek, V., 1981. Characterization of magnetic fabric in rocks. Tectonophysics 79, T63–T67.

Ludman, A., 1999. Constraints on timing and displacement of multistage shearing in the Norumbega Fault System, eastern Maine. Geological Society of America Special Paper 331, 179–194.

Ludman, A., West, D.P. (Eds.), 1999. Norumbega Fault System of the Northern Appalachians. Geological Society of America Special Paper #331, Boulder, CO.

Lux, D.R., Gibson, D., 2000. Magmatic structures within the Mt. Waldo

granite. Abstracts with Programs—Geological Society of America Northeast Section 32, A-32.

Lux, D., Good, M., 2001. Cumulate structures within the Mount Waldo pluton, Maine. Geological Society of America Northeast Section, Abstracts with Programs A-67, Vol. 33, No. 1.

Lux, D.R., Gibson, D., Hogan, J.P., Johnston, B., 2000. Petrologic variation and magmatic structures in plutons of Penobscot Bay area, Maine. New England Intercollegiate Geological Conference 92nd Annual Meeting trip C-2, pp. 208–223.

Osberg, P.H., Hussey, A.M., Boone, G.M., 1985. Bedrock Geologic Map of Maine, Maine Geologic Survey, Augusta.

Paterson, S.R., Fowler, T.K., Schmidt, K.L., Yoshinubo, A.S., Yuan, E.S., Miller, R.B., 1998. Interpreting magmatic fabric patterns in plutons. Lithos 44, 53–82.

Petford, N., Cruden, A.R., McCaffrey, K.J.W., Vigneresse, J.-L., 2000. Granite magma formation, transport and emplacement in the Earth's crust. Nature 408, 669–673.

Robinson, P., Tucker, R.D., Bradley, D., Berry, H.N., Osberg, P.H., 1998. Paleozoic Orogens in New England, USA. GFF 120, 119–148.

Rochette, P., 1987. Magnetic susceptibility of the rock matrix related to magnetic fabric studies. Journal of Structural Geology. 9, 1015–1020.

Rochette, P., Jackson, M., Auborg, C., 1992. Rock magnetism and the interpretation of anisotropy of magnetic susceptibility. Reviews of Geophysics 30, 209–226.

Saint Blanquat, M., Tikoff, B., 1997. Development of magmatic to solid-state fabrics during syntectonic emplacement of the Mono Creek granite, Sierra Nevada Batholith, CA. In: Bouchez, J.L., Hutton, D.W.H., Stephens, W.E. (Eds.), Granite: from Melt Segregation to Emplacement Fabrics. Kluwer, Dordrecht, The Netherlands, pp. 231–252.

Short, H., 2000. Acadian transpression and the exhumation of the sillimanite-bearing Passagassawakeag terrane along the Liberty–Orrington Fault, coastal Maine. Atlantic Geology 35, 27–38.

Stewart, D.B., Unger, J.D., Hutchinson, D.R., 1995. Silurian tectonic history of Penobscot Bay region, Maine. Atlantic Geology 31, 67–79.

Stupavsky, M., 1984. Operating Manual for the SI2B Magnetic Susceptibility and Anisotropy Meter. Sapphire Instruments, Ruthven, ONT.

Swanson, M.T., 1992. Late Acadian–Alleghenian transpressional deformation: evidence from asymmetric boudinage in the Casco Bay area, coastal Maine. Journal of Structural Geology 14, 323–341.

Sweeney, J.F., 1972. Detailed gravity investigation of the shapes of granitic intrusives, South-central Maine, and implications regarding their mode of emplacement. Ph.D., State University of New York at Buffalo.

Sweeney, J.F., 1976. Subsurface distribution of granitic rocks, South-central Maine. Geological Society of America Bulletin 87, 241–249.

Tarling, D.H., Hrouda, F., 1993. The Magnetic Anisotropy of Rocks, Chapman and Hall, London.

Trefethen, J.M., 1944. Mt. Waldo batholith and associated igneous rocks, Waldo County, Maine. Bulletin of the Geological Society of America 55, 895–904.

Uyeda, S., Fuller, M.D., Belshé, J.C., Girdler, R.W., 1963. Anisotropy of magnetic susceptibility of rocks and minerals. Journal of Geophysical Research 68, 279–291.

West, D.P., 1999. The timing of displacements along the Norumbega Fault Zone, south-central and south coastal Maine. Geological Society of America Special Paper 331, 167–178.

West, D.P., Hubbard, M.S., 1997. Progressive localization of deformation during exhumation of a major strike-slip shear zone: Norumbega fault zone, south-central Maine, USA. Tectonophysics 273, 185–201.

West, D.P., Lux, D.R., 1993. Dating mylonitic deformation by the $^{40}Ar/^{39}Ar$ method; an example from the Norumbega fault zone, Maine. Earth and Planetary Science Letters 120, 221–237.

Wones, D.R., 1991. Bedrock Geologic Map of the Bucksport Quadrangle, Waldo, Hancock, and Penobscot Counties, Maine. USGS Geologic Quadrangle Map GQ-1692.